Nanoscale Advances

ROYAL SOCIETY OF CHEMISTRY

PAPER

Cite this: *Nanoscale Adv.*, 2022, **4**, 4391

Wafer-scale MoS_2 with water-vapor assisted showerhead MOCVD†

Michal Macha,*[a] Hyun Goo Ji,[b] Mukesh Tripathi,[b] Yanfei Zhao,[b] Mukeshchand Thakur,[a] Jing Zhang,‡[b] Andras Kis[b] and Aleksandra Radenovic *[a]

Among numerous thin film synthesis methods, metalorganic chemical vapor deposition performed in a showerhead reactor is the most promising one for broad use in scalable and commercially adaptable two-dimensional material synthesis processes. Adapting the most efficient monolayer growth methodologies from tube-furnace systems to vertical-showerhead geometries allows us to overcome the intrinsic process limitations and improve the overall monolayer yield quality. Here, we demonstrate large-area, monolayer molybdenum disulphide growth by combining gas-phase precursor supply with unique tube-furnace approaches of utilizing sodium molybdate pre-seeding solution spincoated on a substrate along with water vapor added during the growth step. The engineered process yields a high-quality, 4-inch scale monolayer film on sapphire wafers. The monolayer growth coverage, average crystal size and defect density were evaluated using Raman and photoluminescence spectroscopy, X-ray photoelectron spectroscopy, scanning electron microscopy and scanning transmission electron microscopy imaging. Our findings provide a direct step forward toward developing a reproducible and large-scale MoS_2 synthesis with commercial showerhead reactors.

Received 24th June 2022
Accepted 1st September 2022

DOI: 10.1039/d2na00409g

rsc.li/nanoscale-advances

1 Introduction

From the broad family of atomically thin, two-dimensional (2D) materials, molybdenum disulphide (MoS_2) has been found particularly interesting in recent years. Being a member of transition metal dichalcogenides (TMDs),[1] the unique electronic[2,3] and optical properties[4] combined with high mechanical flexibility[5,6] of MoS_2 make it an attractive candidate for a potential new generation of wearable devices,[7] flexible sensors[8–10] or nanoelectronics[2,11] as well as heterostructure research and development.[12–20] Therefore, after years of extensive study, the shift of academic focus from small, lab-scale synthesis methods towards prototype applications and scalable processes is inevitable.[21–23]

One of the most vigorously investigated aspects of scaling up the research and application of MoS_2 is large-scale, uniform and high quality material synthesis.[24–32] Over the years, numerous efforts to understand, optimize and grow large-area 2D films have been reported.[22,33] The most researched and versatile approaches are chemical vapor deposition (CVD)[25,30,31,34] and metalorganic chemical vapor deposition (MOCVD) processes,[24,32,35,36] both allowing atomic thickness-controlled growth. While CVD is considered the most common and straightforward method due to the use of commonly available powder precursors of sulfur and molybdenum, its metalorganic MOCVD variant is considered to be crucial to achieve the best results and highest reported material quality.[24]

The most important feature of MOCVD is its high level of repeatability due to the use of gaseous precursors and wide array of tunable process parameters. Recent research showed the potential of MOCVD to obtain high quality monolayer TMD films using hexacarbonyls (*e.g.* molybdenum hexacarbonyl – $Mo(CO)_6$) as a metal source[24,32,35,37] and either diethyl,[35,36] dimethyl[28] or chalcogenide hydrides as the chalcogen precursor (*e.g.* hydrogen disulphide H_2S[24,37]). This, combined with a thorough study of the precursor reactions and thermodynamics, gaseous parameters[38,39] and added growth promoters using liquid salt solutions[28,37,40] proved to be the key to obtaining superior material properties, large crystal size and uniform substrate coverage on large scale substrates.

However, the most promising results in the TMD synthesis field are obtained using the hot-wall, tube furnace geometry. Although a robust and relatively cheap method of 2D material synthesis, tube furnaces do have a significant size limitation prohibiting further fabrication upscaling and industrial adaptation of monolayer MoS_2. Promising studies using much more

[a]*Laboratory of Nanoscale Biology, Institute of Bioengineering, Ecole Polytechnique Federale de Lausanne (EPFL), Lausanne, 1015, Switzerland. E-mail: michal.macha@epfl.ch; aleksandra.radenovic@epfl.ch*

[b]*Laboratory of Nanoscale Electronics and Structures, Electrical Engineering Institute and Institute of Materials Science, Ecole Polytechnique Federale de Lausanne (EPFL), Lausanne, 1015, Switzerland*

† Electronic supplementary information (ESI) available: One table and six figures. See https://doi.org/10.1039/d2na00409g

‡ Current address: State Key Laboratory of Superlattices and Microstructures, Institute of Semiconductors, Chinese Academy of Sciences, Beijing 100083, China.

versatile showerhead systems, typically used in the modern semiconductor's industry[41] for repeatable, large-scale manufacturing, have demonstrated the capability of MoS_2 and other TMD synthesis on a 4-inch wafer scale. Atomic layer deposition (ALD),[42,43] molecular beam epitaxy (MBE)[44,45] and MOCVD approaches[32,46–48] to synthesize TMD monolayers were reported. The material made in such processes however lacks the qualities of tube-furnace monolayers. Due to different furnace geometry (involving a laminar gas flow, shorter distance between the gas inlet and substrate, and heating directly at the substrate susceptor) the most successful tube-furnace methods have not been directly applied with showerhead systems. Instead, thin films reported to date with showerhead reactors show much smaller domain size (from tens of nanometers[32,42,43,46,47] to tens of micrometers[48]) as compared to their tube furnace counterparts, which significantly impact the material properties. The high-temperature decomposition products of organic gaseous precursors tend to contaminate the material with carbonaceous impurities[49] and might lead to growth limiting or suppressing phenomena,[38,39] and thus need to be precisely controlled. On top of that, a typical process suffers from long deposition times, often reaching tens of hours which makes the grown material expensive to obtain.

In this study we revise and compare the state-of-the-art tube-furnace MOCVD methods of large-scale monolayer MoS_2 synthesis: the all-gas-phase process, the use of salt solutions as growth and seeding promoters and the addition of water-vapor are adapted to the showerhead reactor geometry. We optimize these methods and demonstrate for the first time their viability and practical use in an industrial-grade showerhead system. We further engineer the most efficient, combined showerhead MOCVD synthesis approach to achieve uniform, continuous wafer-scale monolayer MoS_2 with the largest reported grain sizes to date (>100 μm). Finally, we show and discuss how the material quality, uniformity and coverage can be dramatically improved by adding water vapor to the process gas mixture to eradicate growth-limiting factors such as carbonaceous and organic gas decomposition products. The results are obtained in an industrial-grade MOCVD system and are supported by systematic Raman and photoluminescence (PL) analysis as well as X-ray photoelectron spectroscopy (XPS) and defect density calculations based on a scanning transmission electron microscope (STEM) study. This work provides a direct methodology to widely adapt large-area, monolayer MoS_2 synthesis to industrial showerhead systems.

2 Experimental results and discussion

All experiments were performed on a commercial Aixtron BM Novo MOCVD system. The coldwall, showerhead reactor is designed to separate the chalcogen and metal precursor sources preventing the premature occurrence of the MOVCD reactions, before reaching the substrate surface (Fig. 1A) minimizing potential unwanted processes and reactor contamination. Such an adaptation is vital for a controlled and clean process reaction since the decomposition temperature of the gaseous molybdenum precursor used here ($Mo(CO)_6$) is relatively low (250 °C (ref. 50)) and may lead to gas lines and showerhead contamination. All MOCVD growth variations are schematically shown in Fig. 1B–E and are discussed in detail in the following sections. All growth experiments are performed under constant parameters of 960 °C, a pressure of 830 mbar, a growth step time of 150 min and by using a 4-inch c-cut sapphire wafer as a growth substrate. Argon is used as an ambient gas and precursor carrier, whereas H_2 is used as an active gas and carbonyl reduction agent. Flow parameters are detailed in Fig. S1† and in the Methods section.

MoS_2 growth with gas-phase precursors

The first investigated MOCVD process pathway for MoS_2 growth is gas-phase synthesis (Fig. 1B). It is considered as a benchmark process as it does exploit all tube-furnace method adaptations discussed further. During gas-phase MOVCD growth, all of the precursors are fed into the reactor chamber through the showerhead along with the carrier gas (argon) and additional process gases (hydrogen) necessary for efficient synthesis of the monolayer film. Although a fundamentally scalable and clean synthesis approach, achieving large lateral MoS_2 domains in the showerhead system is challenging due to the large nucleation density and low reaction rate.[51] The typical crystal size reported in the literature reaches up to 100 nm.[32,43,46] In addition, only material thickness (and not single grain size) scales with the process time. In our optimized method, we have surpassed that limit reaching a size of 500 nm of single crystal monolayer material (Fig. 2A and B) with gas-phase precursors only. It is evident that the crystal size is limited by the reaction byproducts[24,38,39] causing high temperature etching effects as well as high nucleation rate prohibiting the lateral crystal growth. The average substrate surface is thus composed of large crystals mixed with much smaller MoS_2 nuclei, constantly formed and etched during the process (Fig. 2B) by gaseous products of the $Mo(CO)_6/H_2S/H_2$ chemical reaction.[46] On top of that, since the process requires a steady ratio of Mo : S along the entire substrate area, even the smallest flaws or imbalances in the gas feed or showerhead design may cause nonuniform growth conditions leading to uneven crystallization and local growth anomalies. Therefore, achieving stable coverage and substrate-wide uniformity, using this approach, is still challenging and far from the results reported in hotwall MOCVD systems.[24]

MoS_2 growth with coated film sulfurization

Another way of controlling the precursor coverage is to use a liquid source of molybdenum. In this approach, we are spin-coating the substrate with sodium molybdate (Na_2MoO_4) and sodium chloride (NaCl) water solution (Fig. 1C). Such a combination allows pre-seeding[28,35] of the surface with a controlled amount of molybdenum and uniformly coating it with NaCl, widely used in tube furnace MOCVD MoS_2 methods for increasing the reaction rate and decreasing the nucleation density leading to large single crystal formation.[28,35] The coated wafer is then sulfurized under a H_2S gas flow without an external, gaseous source of molybdenum. The material tends to form large single crystals and continuous films, the thickness

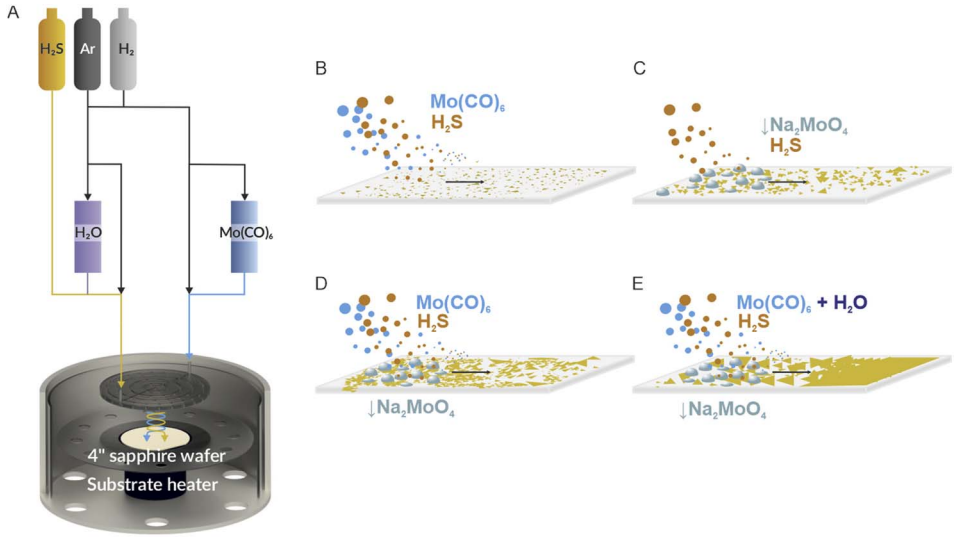

Fig. 1 (A) A schematic of the experimental MOCVD setup with showerhead designed to prevent the chalcogen and metal precursor sources from mixing prematurely before reaching the reactor volume. With the gas-phase only approach (B), a liquid-phase-sulfurization approach (C), hybrid gas + liquid growth method (D) and a H_2O assisted growth method with a controlled supply of the moderate amount of H_2O vapor (E).

and coverage of which depend on the spincoated mixture concentration, which controls the local Mo saturation during growth. The Na_2MoO_4/NaCl sulfurization approach was demonstrated to be efficient for continuous monolayer growth on 1–3 inch substrates;[35,36] however the use of the alkali salt solution heavily impacts the final material quality. Intermediary

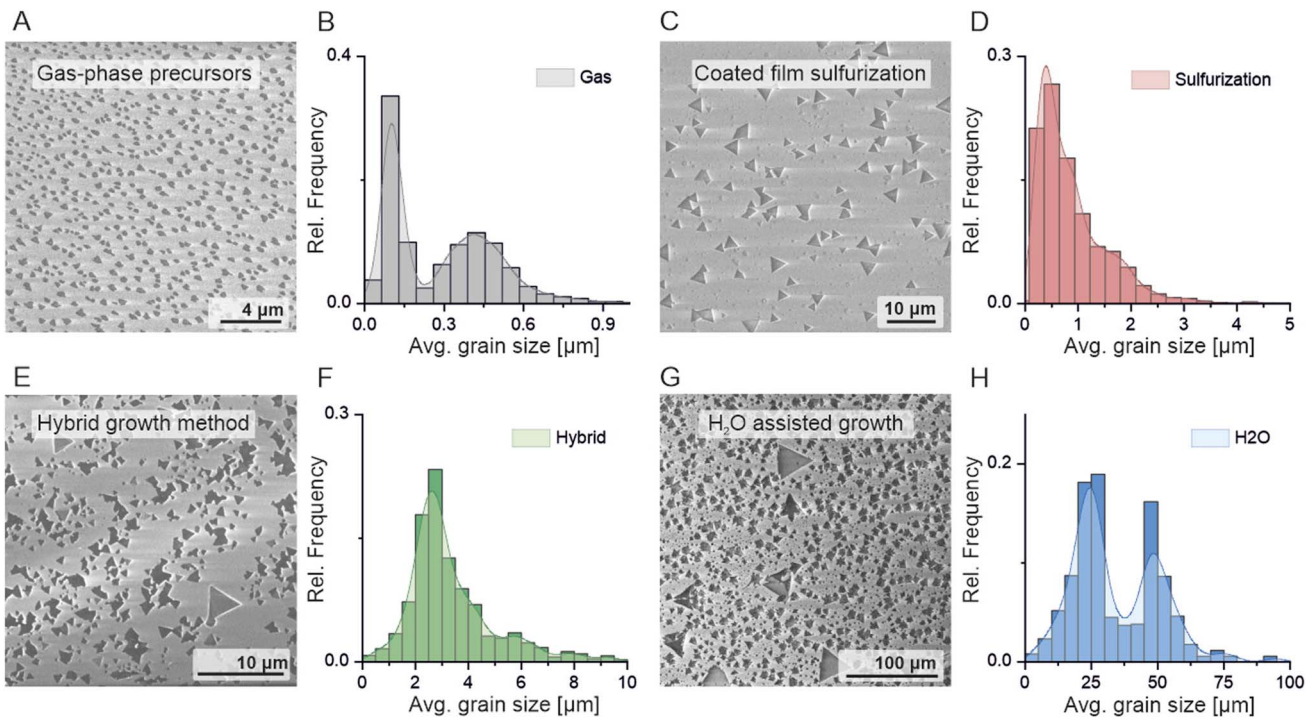

Fig. 2 A comparison of the MoS_2 growth yield obtained through different growth approaches. The SEM image analysis of the gas-phase only approach (A) shows small, densely nucleated grain clusters with an average size of 500 nm and large contribution from unripened nuclei (B). A coated-film sulfurization approach yields large, 1 μm crystals which locally reach up to 3–4 μm (C) and (D). The hybrid growth method results in an average of 3 μm single crystals (E) and (F). Finally, with a controlled supply of the moderate amount of H_2O vapor the lateral crystal size increases by an order of magnitude (G) and (H) with evident separation between two combined growth regimes (liquid and gas phases) visible in the grain size distribution (H). The presented SEM images were chosen from the substrates' edge to show an av. grain size. Histograms were obtained from 20 separate SEM images from each growth method.

NaCl + MoS_2 reaction products[52] lead to a fast crystal growth rate but also have been found to remain underneath MoS_2 films. This phenomenon, driven by excessive use of NaCl, negatively impacts the epitaxial connection between the crystal and sapphire substrate and may lead to grain boundary defects and uneven grain stitching inherently deteriorating large-area continuous film cohesion and its electronic parameters.[52] To avoid this unwanted effect, we have limited the Na_2MoO_4/NaCl molar concentration to 0.03 M and 0.1 M respectively. This allowed the preservation of the MoS_2/sapphire epitaxy and maintenance of high material coverage. In our coldwall, showerhead regime, we note lateral crystal size varying from 0.7 up to 3–4 μm (Fig. 2C and D) with sporadic events of >100 μm single crystals forming continuous films locally. This growth method has an intrinsic self-limiting character due to a fixed amount of Mo coated on the substrate. Tuning the precursor solution molar concentration allows the control over the coverage and nucleation density; however uniformity is problematic on large area substrates. The uneven film thickness inherent to the spin-coating process (especially emphasized in large-scale growth areas) leads to different local Mo : S concentrations during the process. Such a coverage issue is manifested in bilayer, multilayer or blank areas with the presence of unreacted, bulk molybdenum oxide particles on different substrate areas. The sulfurization of the spincoated Na_2MoO_4/NaCl film is therefore not perfectly adjustable in the case of 4-inch substrates and requires careful molar concentration to balance between preserving epitaxy and promoting continuous film growth to be useable.

MoS_2 growth with a hybrid process

Increasing the control over the material's coverage, crystal density and uniformity even further requires finetuning the precursor flux *i.e.* by combining two precursor sources: adding a gas phase $Mo(CO)_6$ flow to the process with a spincoated mixture of Na_2MoO_4/NaCl (Fig. 1D) on the substrate. The combined, hybrid method in principle allows the compensation of individual limitations of small grain size present in the gas phase method and self-limiting Mo supply of the spincoated film sulfurization approach. In this case, we consider Na_2MoO_4/NaCl as a Mo seeding/catalytic agent, leading to the formation of molybdenum oxychlorides, oxysulfides and suboxides[28] kickstarting and promoting the film growth under the constant supply of Mo from the $Mo(CO)_6$ gas phase. Indeed, in our experiments the hybrid method yields single crystals of 3 μm average lateral size (Fig. 2E and F) with the largest exceeding 100 μm locally. Adding $Mo(CO)_6$ however reintroduces the carbonyl reaction byproducts from the $Mo(CO)_6$ + H_2S + H_2 reaction. Further optimization of the process (to improve the single crystal size, uniformity and monolayer coverage) does not intuitively scale with the $Mo(CO)_6$ nor Na_2MoO_4/NaCl concentration during the growth. The local imbalances of Na_2MoO_4 and $Mo(CO)_6$ lead to multilayer island formation. We have found that reducing the molar concentration of Na_2MoO_4 to as low as 0.005 M is enough to effectively pre-seed and nucleate Mo_2 and crucial to minimize the multilayer growth under a constant $Mo(CO)_6$ mass flux. As discussed later, in our experiments volatile carbonaceous reaction products (CO_2 and CH_4, C) do not seem to dope MoS_2 nor contaminate the substrate; however they do contaminate the showerhead and MOCVD reactor heavily, significantly suppressing the growth process by releasing carbonaceous products into the gas phase growth environment limiting the reproducibility. Thus, further increase of $MoCO_6$ concentration is unwelcome and counter-productive for obtaining high-quality, large-area films. The scalability of the hybrid approach offers more process parameters and better coverage control; however it still requires significant optimization to be viable on an industrial scale.

Water-assisted large grain growth

The presence of water vapor during the MOCVD reaction is widely considered as unwanted. Uncontrollable moisture can lead to a significant decrease of material quality due to water-induced oxidation and reduction during the growth process.[53] However, as was previously reported in tube-furnace, small scale processes, controlled addition of a small amount of water vapor was found to be beneficial due to low oxidizing effects, which assist in the removal of volatile carbonaceous reaction products[48,54] and assists in the reduction of molybdenum oxides to suboxides and hydrogen promoting the lateral growth (formulas (1)–(3))

$$C + H_2O \Rightarrow CO + H_2 \quad (1)$$

$$MoO_3 + H_2 \Rightarrow MoO_{3-x} + H_2O \quad (2)$$

$$MoO_{3-x} + (7 - x)2S \Rightarrow MoS_2 + (3 - x)/2SO_2 \quad (3)$$

The use of oxidizing materials such as water vapor in an industrial-grade showerhead reactor is in general significant safety concern. However, by maintaining proper safety precautions and source separation we have achieved a water-assisted method combining metalorganic gas supply and promoter film coating (Fig. 1E). We found that a flow of 5 sccm of argon through a room temperature H_2O filled bubbler is sufficient to significantly remove impurities and promote monolayer crystals to reach an average lateral size of 25–50 μm (Fig. 2G and H) with the largest locally exceeding 100 μm (Fig. 3) and with a significant increase in continuous film coverage with further increase in the water vapor flow. The monolayer coverage peaked at a H_2O vapor flow of 20 sccm (Fig. 3D and E) and its continuity was maintained across a 4-inch substrate area (Fig. 3D) with the exception of the substrate edge (see Fig. S2†). We attribute this dramatic improvement of the crystal size and monolayer coverage to the self-regulating effect of H_2O, similar to the growth-etch approach demonstrated in tungsten disulphide (WS_2) pulsed MOCVD process.[48] Due to gas-flow imbalances coming from subtle showerhead and gas-line imperfections as well as coated film non-uniformity (amplified by the large-area substrate), different $Mo(CO)_6$ + H_2S + H_2 reaction pathways may occur locally leading to the formation of volatile CH_4, C, CO, CO_2, COS, and CS_2 species in different concentrations.[38,46] Water vapor may react with and suppress the formation of

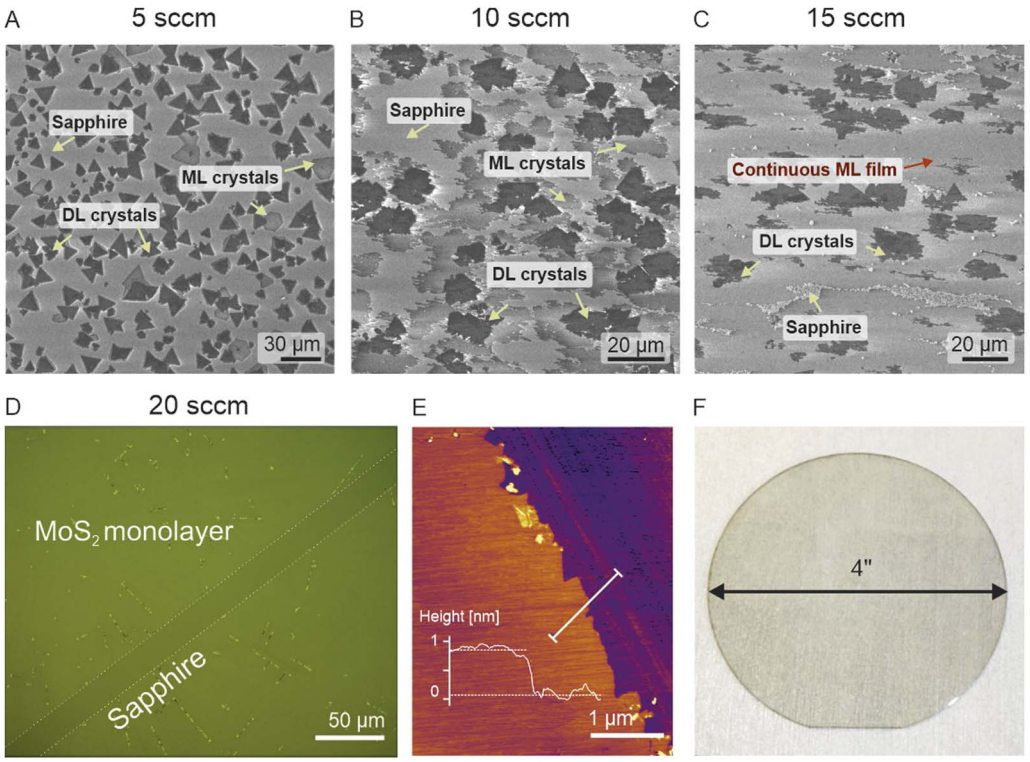

Fig. 3 SEM images of MoS_2 coverage with increasing H_2O vapor concentration during the growth process. Coverage of the continuous monolayer (ML) film improves gradually with the increase in the water vapor supply (A)–(C) and peaks at 20 sccm where a continuous ML film without double layer (DL) crystals is observed as shown on panel (D) (optical microscope image of the deliberately scratched MoS_2 film). Local AFM analysis confirms the monolayer thickness (E). Material uniformity is maintained over the 4-inch substrate area (F).

excess carbon oxides and sulfides negating the effects of local differences in reaction paths and their negative impact on MoS_2 grain lateral growth leading to overall better coverage as shown in Fig. 3D and E.

Spectroscopic characterization

Detailed material characterization was performed to compare the uniformity and crystallinity of MoS_2 synthesized by each growth approach. The analysis of the shape of characteristic E_{2g} and A_{1g} Raman peaks from monolayer areas from each method (Fig. S3A†) shows $\Delta_{E_{2g}-A_{1g}}$ to be 20.9, 20.8 and 19.5 for sulfurization, hybrid and H_2O respectively. The gas-phase growth method proved to be difficult to analyze due to the small grain size and low Raman signal. The full width at half maximum (FWHM) of E_{2g} and A_{1g} of each method is shown in Fig. S3B† and it was found to be narrowest for the H_2O assisted approach with an E_{2g} and A_{1g} of 2.6 and 3.4, indicating higher crystallinity and good uniformity. In the case of all substrates, spectra taken from the 1000–1700 cm^{-1} range showed no distinguishable carbon peaks (Fig. S4†), which suggests that all carbonaceous reaction products remain in the gas phase and do not deposit on the substrate. Raman spectra taken radially from 50 spots on each wafer confirm the self-regulating effect of H_2O (Fig. 4A). The separation between E^1_2g and A_{1g} peaks smaller than 20 cm^{-1} is regarded as a proof of a high-quality monolayer[55] film. The positions of Raman peaks in the case of water-assisted growth remain constant which indicates uniformity in thickness and strain compared with other growth methods. Water vapor can promote further oxidation of thick particles from residual Mo oxides and etching of emerging multilayers during the growth process due to local H_2 generation (as presented in formulas (1)–(3)). The result is the formation of a continuous monolayer film without thicker, seed particles on a wide area of the 4-inch substrate. Panel 4B shows the PL spectra of MoS_2 synthesized with sulfurization (red), hybrid (green) and H_2O assisted (blue) methods taken from the monolayer MoS_2 sites from each substrate. Significantly higher PL emission from water assisted growth indicates that water improves crystal quality by removing carbon contamination (which is known to quench PL[54]) and enhances the efficiency of precursor ligand-reduction. The increase in PL intensity signifies a lower impact of grain boundary defects and uneven grain stitching.[56] In this case, the obtained Raman and PL spectra are evidence of a high quality, large-area film cohesion obtained with the water-assisted growth method through large crystals and potentially epitaxial grain stitching.

XPS analysis

An XPS measurement was performed to investigate the chemical states and stoichiometric ratio of the grown MoS_2. Trace sodium was only detected on liquid-phase sulfurized MoS_2 substrates (Fig. 4C and Table S1†) as this process relies on coating the substrate with relatively concentrated Na_2MoO_4/NaCl solution compared to the hybrid approach (0.03/0.1 M as compared to 0.005/0.1 M). The detailed atomic ratios, molybdenum oxides

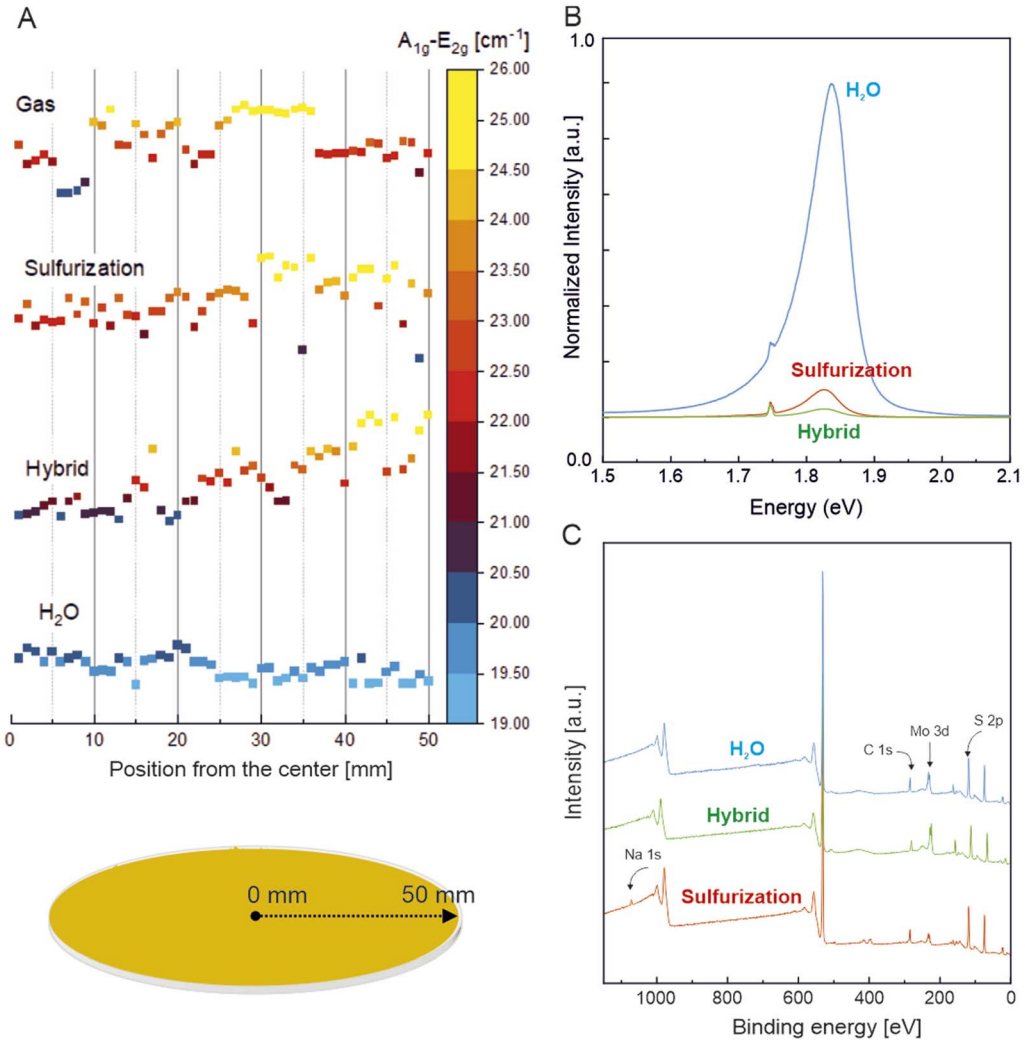

Fig. 4 An average separation of E_{2g} and A_{1g} Raman peaks taken from 50 measurements with a 1 mm interval performed across the radial direction of the wafer (A). Measurements were performed in a line-scan fashion, from the center to the edge of the 4-inch substrate. Comparison of characteristic Raman peak separation shows the radial uniformity of MoS_2 synthesised with the water-vapor assisted growth method. Representative PL spectra (B) showing significantly higher PL emission from water assisted growth. A comparison of wide XPS spectra (C) shows no residual Na present with H_2O assisted growth. Detailed analysis of Mo 3d and S 2p XPS peaks is shown in ESI Fig. S5.†

and sodium contents of each growth method are shown in ESI Table S1.† The analysis of the atomic ratios of each growth method reveals the sulfurization method to yield an ≈2.22 Mo : S ratio, as compared to ≈6.1 for the hybrid and ≈3.4 for the H_2O approach. However, compared to other growth methods, the H_2O assisted method produces the least oxide states (Fig. S5A and C†), attributed to the Mo^{6+} ratio. It is explained by water-assisted enhanced reduction of the metal precursor, which results in higher crystallinity. The lack of detected sodium within the measurement limit in the water-assisted method combined with the obtained Raman spectroscopy results discussed in the previous paragraph suggests the high quality of the monolayer material synthesized in this process approach.

STEM imaging

Aberration-corrected STEM imaging was used to image and characterize the structural properties of MoS_2 at atomic resolution. Small and large magnified high angle annular dark field (HAADF) images (Fig. 5A and B) show a clean and perfect hexagonal crystal lattice of the monolayer MoS_2 film in the 2H phase. Due to the *Z*-contrast dependency of HAADF, the atomic intensities of Mo and 2S can be distinguished directly from the atomically resolved images (Fig. 5C). In the case of earlier reported exfoliated and MOCVD grown monolayer MoS_2, different types of defects have been reported. However, here only sulfur mono- and divacancies can be observed which are very common due to their lower formation energies. Moreover, an electron beam can also induce sulfur defects even at lower acceleration voltages. Thus to extract the intrinsic S defect concentrations, the number of mono- and divacancies can be calculated with respect to the accumulated electron beam dose in an image series.[57] Further defect concentration analysis shows a pristine defect concentration of 1.4×10^{13} cm^{-2} for single sulfur vacancies (V_S) and 0.3×10^{13} cm^{-2} for double sulfur vacancies

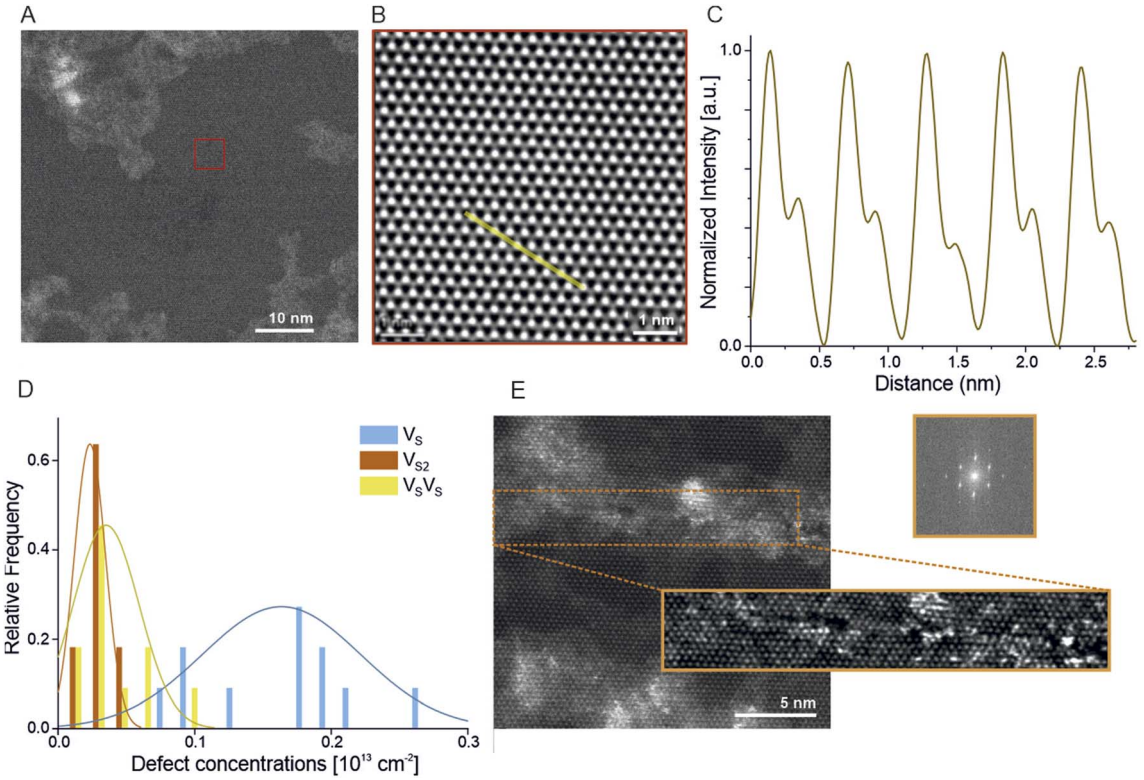

Fig. 5 A small magnification STEM image (A) of MoS_2 synthesized with the water-assisted method with a large magnification image of the typical MoS_2 area (B) (marked in red) with an intensity line-section (C) showing high crystal quality. Typical defect concentration is presented in the bar plot (D) and it is calculated separately for single sulfur V_S, double sulfur V_{2S} and sulfur-next-to-sulfur V_SV_S defect types. Concentrations are calculated from the 16 images taken from different regions. A grain boundary image (E) and its closer inspection show seamless grains stitching (FFT), a sign of local epitaxial growth mode.

(V_{2S}) as extrapolated from an E-beam dose rate test (Fig. S6†). A distribution of V_S, V_{2S} and sulfur-next-to-sulfur (V_SV_S) defects taken from 11 STEM images (measured area of 925 nm^2) is presented in Fig. 5E. MoS_2 synthesized in the water-assisted process does not show any signs of unwanted etching or oxidative damage. Interestingly, the grain boundaries found during imaging are stitched seamlessly (Fig. 5E), demonstrating locally the epitaxial growth mode. Due to the reactive nature of grain boundaries, they tend to attract contamination along it. However, the filtered STEM image (highlighted in orange color) shows no disorientation angle between the stitched crystal areas. The fast Fourier transform (FFT) of the corresponding image shows only one set of hexagonal patterns, further confirming the high-quality growth of MoS_2.

3 Conclusion

All experimental evidence points to a strong advantage of combining the hybrid gas and liquid phase growth approaches in a coldwall showerhead system. We have successfully achieved a uniform and continuous MoS_2 film over a large scale 4-inch substrate with spincoated Na_2MoO_4/NaCl solution and gas-phase $Mo(CO)_6$ and H_2S by limiting growth reaction imbalances with water vapor introduced during the growth phase. We found that the water regulates the growth reaction by removing carbonaceous products and reduces excess molybdenum oxides. Material characterization confirms the good material quality and no negative impact of using moderate and carefully controlled amounts of H_2O.

The synthesized MoS_2 showed evidence of epitaxial connection with the sapphire substrate. Our findings provide a direct step forward towards developing scalable, reproducible and large-scale MoS_2 synthesis with showerhead reactors and demonstrate the potential of combining key advancements in the field of 2D material growth to overcome the process limitations.

4 Methods

MOCVD growth

All MoS_2 synthesis experiments were performed on an Aixtron BM Novo MOCVD system with a coldwall, showerhead, horizontal growth chamber. Prior to growth, 4-inch *c*-plane sapphire wafers (MTI) were cleaned in IPA, acetone and DI and annealed at 1000 °C for 6 h to obtain an atomically smooth surface. For sulfurization, hybrid and H_2O assisted growth methods, a sapphire wafer was additionally treated in 50 W O_2 plasma for 5 min to ensure a hydrophilic surface needed for efficient spincoating of a growth promoter (a solution of Na_2MoO_4 (Sigma Aldrich, 98.0%) and NaCl (Sigma Aldrich, 99.5%) in DI with

concentrations of 0.03 M/0.1 M for sulfurization and 0.005 M/0.1 M for hybrid and H_2O). All growth processes started with heating the reactor with a sapphire wafer to 950 °C in 60 min under a constant flow of 300 sccm of high purity argon (Carbagas 99.999%). The growth step started immediately after reaching the set temperature. All substrates were exposed to 20 sccm of hydrogen gas (Vici DBS NM Plus 100 Hydrogen Generator, purity 99.999%) and 60 sccm of H_2S (Carbagas, 99.9%). For gas-phase, hybrid and H_2O assisted approaches, $Mo(CO)_6$ (Sigma Aldrich 99.9%) was supplied by 150 sccm of Ar gas flowing through a bubbler kept at 10 °C. In the H_2O assisted variant, an additional 5–20 sccm of Ar flowing through a DI-filled bubbler at room temperature was introduced. All MoS_2 growths were done at 830 mbar with growth steps set to 150 min (although the sulfurization method was completed in only 30 min). After that, the reactor was cooled under ambient H_2S and Ar flows. After a growth run, the reactor chamber was thoroughly cleaned and annealed and all the ceramic elements were additionally air-baked to prevent unwanted carbon contamination.

Raman spectroscopy and PL

Raman and PL spectroscopy were done with a Renishaw inVia Confocal Raman Microscope with a 532 nm laser beam at a low power (<0.3 mW) to avoid defect nucleation and substrate damage. A diffraction grating of 3000 mm^{-1} was used for good spatial resolution.

Atomic force microscopy

Atomic force microscopy was performed on an Asylum Research Cypher AFM system in tapping mode.

SEM imaging

Scanning electron microscopy was done on a Zeiss Merlin SEM with a GEMINI II column. All imaging was done at 1 kV acceleration voltage to minimize substrate charging STEM imaging. The as-grown MoS_2 was transferred from the growth substrate using the wet-transfer method[36] on 5 × 5 mm Si/SiN TEM grids (Norcada). Scanning transmission electron microscopy imaging was conducted using an aberration-corrected (with a double spherical corrector) FEI Titan Themis TEM 60–300 kV, equipped with a Schottky X-FEG electron source and a monochromator to reduce the effect of chromatic aberrations. To avoid the electron-beam induced knock-on damage, a low acceleration voltage (80 kV) was used for the imaging.[58] The electron probe current, C_2 aperture size, and beam convergence angle were 25 pA, 50 μm, and 21.2 mrad, respectively. Images were acquired with Velox software (Thermo Fisher Scientific) using a 185 mm camera length, which corresponds to an angular range (49.5–198 mrad) in a HAADF detector. To avoid the sample drift, serial imaging was performed using 512 × 512 pixels with an 8 μs dwell time. The images were aligned and processed using the "double-Gaussian filtering" method in ImageJ.

Author contributions

A. R., A. K. and M. M. conceived and designed the experiments; M. M. synthesized the samples and optimized the process, M. M., H. G. J., Y. Z. and J. Z. developed the process parameters, M. M. performed the optical, SEM, HRTEM, Raman and PL measurements, H. G. J. and M. M. analyzed the data, M. Thakur transferred the substrates on TEM grids, and M. Tripathi obtained and analyzed the STEM images. M. M. wrote the paper, with inputs from all authors; A. K. and A. R. supervised the project; all authors discussed the results and commented on the manuscript.

Conflicts of interest

The authors declare no competing financial interest.

Acknowledgements

We thank the Aixtron team for technical assistance. This work was financially supported by the Swiss National Science Foundation (grant no. 200021_192037), the CCMX Materials Challenge grant "Large area growth of 2D materials for device integration", the European Union's Horizon 2020 research and innovation program under grant agreements No. 785219 and 881603 (Graphene Flagship Core 2 and Core 3) and the European Research Council (grant no. 682332 and 899775).

References

1 S. Manzeli, D. Ovchinnikov, D. Pasquier, O. V. Yazyev and A. Kis, 2D transition metal dichalcogenides, *Nat. Rev. Mater.*, 2017, **2**(8), 1–15, DOI: **10.1038/natrevmats.2017.33**.

2 B. Radisavljevic, A. Radenovic, J. Brivio, V. Giacometti and A. Kis, Single-layer MoS_2 transistors, *Nat. Nanotechnol.*, 2011, **6**, 147–150, DOI: **10.1038/nnano.2010.279**.

3 H.-P. Komsa and A. V. Krasheninnikov, Effects of confinement and environment on the electronic structure and exciton binding energy of MoS_2 from first principles, *Phys. Rev. B: Condens. Matter Mater. Phys.*, 2012, **86**(24), 241201, DOI: **10.1103/PhysRevB.86.241201**.

4 A. Splendiani, L. Sun, Y. Zhang, T. Li, J. Kim, C.-Y. Chim, G. Galli and F. Wang, Emerging Photoluminescence in Monolayer MoS_2, *Nano Lett.*, 2010, **10**(4), 1271–1275, DOI: **10.1021/NL903868W**.

5 A. Castellanos-Gomez, M. Poot, G. A. Steele, H. S. J. v. d. Zant, N. Agraït and G. Rubio-Bollinger, Elastic Properties of Freely Suspended MoS_2 Nanosheets, *Adv. Mater.*, 2012, **24**(6), 772–775, DOI: **10.1002/ADMA.201103965**.

6 J.-W. Jiang, H. S. Park and T. Rabczuk, Molecular dynamics simulations of single-layer molybdenum disulphide (MoS_2): Stillinger-Weber parametrization, mechanical properties, and thermal conductivity, *J. Appl. Phys.*, 2013, **114**(6), 064307, DOI: **10.1063/1.4818414**.

7 E. Singh, P. Singh, K. S. Kim, G. Y. Yeom and H. S. Nalwa, Flexible Molybdenum Disulfide (MoS_2) Atomic Layers for Wearable Electronics and Optoelectronics, *ACS Appl. Mater.*

Interfaces, 2019, **11**(12), 11061–11105, DOI: 10.1021/ACSAMI.8B19859.

8 J. Yoon, W. Park, G. Y. Bae, Y. Kim, H. S. Jang, Y. Hyun, S. K. Lim, Y. H. Kahng, W. K. Hong, B. H. Lee and H. C. Ko, Highly Flexible and Transparent Multilayer MoS_2 Transistors with Graphene Electrodes, *Small*, 2013, **9**(19), 3295–3300, DOI: 10.1002/SMLL.201300134.

9 H. Singh Nalwa, A review of molybdenum disulfide (MoS_2) based photodetectors: from ultra-broadband, self-powered to flexible devices, *RSC Adv.*, 2020, **10**(51), 30529–30602, DOI: 10.1039/D0RA03183F.

10 Y. H. T. JA Rogers, Someya: materials and mechanics for stretchable electronics, *Science*, 2010, **327**(5973), 1603–1607, DOI: 10.1126/science.1182383.

11 S. Wachter, D. K. Polyushkin, O. Bethge and T. Mueller, A microprocessor based on a two-dimensional semiconductor, *Nat. Commun.*, 2017, **8**(1), 1–6, DOI: 10.1038/ncomms14948.

12 B. Cho, J. Yoon, S. K. Lim, A. R. Kim, D.-H. Kim, S.-G. Park, J.-D. Kwon, Y.-J. Lee, K.-H. Lee, B. H. Lee, H. C. Ko and M. G. Hahm, Chemical Sensing of 2D Graphene/MoS_2 Heterostructure Device, *ACS Appl. Mater. Interfaces*, 2015, **7**(30), 16775–16780, DOI: 10.1021/ACSAMI.5B04541.

13 S. Rathi, I. Lee, D. Lim, J. Wang, Y. Ochiai, N. Aoki, K. Watanabe, T. Taniguchi, G.-H. Lee, Y.-J. Yu, P. Kim and G.-H. Kim, Tunable Electrical and Optical Characteristics in Monolayer Graphene and Few-Layer MoS_2 Heterostructure Devices, *Nano Lett.*, 2015, **15**(8), 5017–5024, DOI: 10.1021/ACS.NANOLETT.5B01030.

14 D. S. Schulman, A. J. Arnold, A. Razavieh, J. Nasr and S. Das, The Prospect of Two-Dimensional Heterostructures: A Review of Recent Breakthroughs, *IEEE Nanotechnology Magazine*, 2017, **11**(2), 6–17, DOI: 10.1109/MNANO.2017.2679240.

15 G. Swain, S. Sultana and K. Parida, A review on vertical and lateral heterostructures of semiconducting 2D-MoS_2 with other 2D materials: a feasible perspective for energy conversion, *Nanoscale*, 2021, **13**(22), 9908–9944, DOI: 10.1039/D1NR00931A.

16 Z. Cai, B. Liu, X. Zou and H.-M. Cheng, Chemical Vapor Deposition Growth and Applications of Two-Dimensional Materials and Their Heterostructures, *Chem. Rev.*, 2018, **118**(13), 6091–6133, DOI: 10.1021/ACS.CHEMREV.7B00536.

17 G. Eda, T. Fujita, H. Yamaguchi, D. Voiry, M. Chen and M. Chhowalla, Coherent Atomic and Electronic Heterostructures of Single-Layer MoS_2, *ACS Nano*, 2012, **6**(8), 7311–7317, DOI: 10.1021/NN302422X.

18 Y. Liu, N. O. Weiss, X. Duan, H.-C. Cheng, Y. Huang and X. Duan, Van der Waals heterostructures and devices, *Nat. Rev. Mater.*, 2016, **1**(9), 1–17, DOI: 10.1038/natrevmats.2016.42.

19 A. Geim and I. Grigorieva, Van der Waals heterostructures, *Nature*, 2013, **499**(7459), 419–425, DOI: 10.1038/nature12385.

20 J. Sitek, J. Plocharski, I. Pasternak, A. P. Gertych, C. Mcaleese, B. R. Conran, M. Zdrojek and W. Strupinski, Substrate-Induced Variances in Morphological and Structural Properties of MoS_2 Grown by Chemical Vapor Deposition on Epitaxial Graphene and SiO_2, *ACS Appl. Mater. Interfaces*, 2020, **12**, 45110, DOI: 10.1021/acsami.0c06173.

21 M. Shrivastava and V. R. Rao, A Roadmap for Disruptive Applications and Heterogeneous Integration Using Two-Dimensional Materials: State-of the-Art and Technological Challenges, *Nano Lett.*, 2021, **21**(15), 6359–6381, DOI: 10.1021/ACS.NANOLETT.1C00729.

22 S.-Y. Kim, J. Kwak, C. V. Ciobanu and S.-Y. Kwon, Recent Developments in Controlled Vapor-Phase Growth of 2D Group 6 Transition Metal Dichalcogenides, *Adv. Mater.*, 2019, **31**(20), 1804939, DOI: 10.1002/ADMA.201804939.

23 P. Wang, D. Yang and X. Pi, Toward Wafer-Scale Production of 2D Transition Metal Chalcogenides, *Adv. Electron. Mater.*, 2021, **7**, 2100278, DOI: 10.1002/AELM.202100278.

24 K. Kang, S. Xie, L. Huang, Y. Han, P. Y. Huang, K. F. Mak, C.-J. Kim, D. Muller and J. Park, High-mobility three-atom-thick semiconducting films with wafer-scale homogeneity, *Nature*, 2015, **520**(7549), 656–660, DOI: 10.1038/nature14417.

25 H. Yu, M. Liao, W. Zhao, G. Liu, X. J. Zhou, Z. Wei, X. Xu, K. Liu, Z. Hu, K. Deng, S. Zhou, J.-A. Shi, L. Gu, C. Shen, T. Zhang, L. Du, L. Xie, J. Zhu, W. Chen, R. Yang, D. Shi and G. Zhang, Wafer-Scale Growth and Transfer of Highly-Oriented Monolayer MoS_2 Continuous Films, *ACS Nano*, 2017, **11**(12), 12001–12007, DOI: 10.1021/ACSNANO.7B03819.

26 D. Dumcenco, D. Ovchinnikov, K. Marinov, P. Lazić, M. Gibertini, N. Marzari, O. L. Sanchez, Y.-C. Kung, D. Krasnozhon, M.-W. Chen, S. Bertolazzi, P. Gillet, A. F. i. Morral, A. Radenovic and A. Kis, LargeArea Epitaxial Monolayer MoS_2, *ACS Nano*, 2015, **9**(4), 4611–4620, DOI: 10.1021/ACSNANO.5B01281.

27 P. Yang, X. Zou, Z. Zhang, M. Hong, J. Shi, S. Chen, J. Shu, L. Zhao, S. Jiang, X. Zhou, Y. Huan, C. Xie, P. Gao, Q. Chen, Q. Zhang, Z. Liu and Y. Zhang, Batch production of 6-inch uniform monolayer molybdenum disulfide catalyzed by sodium in glass, *Nat. Commun.*, 2018, **9**(1), 1–10, DOI: 10.1038/s41467-018-03388-5.

28 S. Boandoh, S. H. Choi, J.-H. Park, S. Y. Park, S. Bang, M. S. Jeong, J. S. Lee, H. J. Kim, W. Yang, J.-Y. Choi, S. M. Kim and K. K. Kim, A Novel and Facile Route to Synthesize Atomic-Layered MoS_2 Film for Large-Area Electronics, *Small*, 2017, **13**(39), 1701306, DOI: 10.1002/SMLL.201701306.

29 S. Boandoh, F. O. T. Agyapong-Fordjour, S. H. Choi, J. S. Lee, J. H. Park, H. Ko, G. Han, S. J. Yun, S. Park, Y. M. Kim, W. Yang, Y. H. Lee, S. M. Kim and K. K. Kim, Wafer-Scale van der Waals Heterostructures with Ultraclean Interfaces via the Aid of Viscoelastic Polymer, *ACS Appl. Mater. Interfaces*, 2019, **11**(1), 1579–1586, DOI: 10.1021/ACSAMI.8B16261.

30 Q. Wang, N. Li, J. Tang, J. Zhu, Q. Zhang, Q. Jia, Y. Lu, Z. Wei, H. Yu, Y. Zhao, Y. Guo, L. Gu, G. Sun, W. Yang, R. Yang, D. Shi and G. Zhang, Wafer-Scale Highly Oriented Monolayer MoS_2 with Large Domain Sizes, *Nano Lett.*,

2020, **20**(10), 7193–7199, DOI: 10.1021/ACS.NANOLETT.0C02531.

31 T. He, Y. Li, Z. Zhou, C. Zeng, L. Qiao, C. Lan, Y. Yin, C. Li and Y. Liu, Synthesis of large-area uniform MoS_2 films by substrate-moving atmospheric pressure chemical vapor deposition: from monolayer to multilayer, *2D Materials*, 2019, **6**(2), 025030, DOI: 10.1088/2053-1583/AB0760.

32 T. Kim, J. Mun, H. Park, D. Joung, M. Diware, C. Won, J. Park, S.-H. Jeong and S.-W. Kang, Wafer-scale production of highly uniform two-dimensional MoS_2 by metal-organic chemical vapor deposition, *Nanotechnology*, 2017, **28**(18), DOI: 10.1088/1361-6528/AA6958.

33 J. Sun, X. Li, W. Guo, M. Zhao, X. Fan, Y. Dong, C. Xu, J. Deng and Y. Fu, Synthesis Methods of Two-Dimensional MoS_2: A Brief Review, *Crystals*, 2017, **7**(7), 198, DOI: 10.3390/CRYST7070198.

34 Y.-C. Lin, Wafer-scale MoS_2 thin layers prepared by MoO_3 sulfurization, *Nanoscale*, 2012, **4**(20), 6637–6641, DOI: 10.1039/c2nr31833d.

35 H. Cun, M. Macha, H. Kim, K. Liu, Y. Zhao, T. LaGrange, A. Kis and A. Radenovic, Wafer-scale MOCVD growth of monolayer MoS_2 on sapphire and SiO_2, *Nano Res.*, 2019, **12**(10), 2646–2652, DOI: 10.1007/S12274-019-2502-9.

36 M. Thakur, M. Macha, A. Chernev, M. Graf, M. Lihter, J. Deen, M. Tripathi, A. Kis and A. Radenovic, Wafer-Scale Fabrication of Nanopore Devices for Single-Molecule DNA Biosensing Using MoS_2, *Small Methods*, 2020, **4**(11), 2000072, DOI: 10.1002/SMTD.202000072.

37 H. Kim, D. Ovchinnikov, D. Deiana, D. Unuchek and A. Kis, Suppressing nucleation in metal-organic chemical vapor deposition of MoS_2 monolayers by alkali metal halides, *Nano Lett.*, 2017, **17**(8), 5056–5063, DOI: 10.1021/acs.nanolett.7b02311.

38 S. Dhar, V. K. Kumar, T. H. Choudhury, S. A. Shivashankar and S. Raghavan, Chemical vapor deposition of MoS_2 layers from Mo–S–C–O–H system: thermodynamic modeling and validation, *Phys. Chem. Chem. Phys.*, 2016, **18**(22), 14918–14926, DOI: 10.1039/C6CP01617K.

39 V. K. Kumar, S. Dhar, T. H. Choudhury, S. A. Shivashankar and S. Raghavan, A predictive approach to CVD of crystalline layers of TMDs: the case of MoS_2, *Nanoscale*, 2015, **7**(17), 7802–7810, DOI: 10.1039/C4NR07080A.

40 J.-G. Song, G. H. Ryu, Y. Kim, W. J. Woo, K. Y. Ko, Y. Kim, C. Lee, I.-K. Oh, J. Park, Z. Lee and H. Kim, Catalytic chemical vapor deposition of large-area uniform two-dimensional molybdenum disulfide using sodium chloride, *Nanotechnology*, 2017, **28**(46), 465103, DOI: 10.1088/1361-6528/AA8F15.

41 Z. C. Feng, *III-Nitride Semiconductor Materials*, 2006, DOI: 10.1142/P437.

42 Y. Jang, S. Yeo, H. B. R. Lee, H. Kim and S. H. Kim, Wafer-scale, conformal and direct growth of MoS_2 thin films by atomic layer deposition, *Appl. Surf. Sci.*, 2016, **365**, 160–165, DOI: 10.1016/J.APSUSC.2016.01.038.

43 J. Lin, S. Monaghan, N. Sakhuja, F. Gity, R. K. Jha, E. M. Coleman, J. Connolly, C. P. Cullen, L. A. Walsh, T. Mannarino, M. Schmidt, B. Sheehan, G. S. Duesberg, N. McEvoy, N. Bhat, P. K. Hurley, I. M. Povey and S. Bhattacharjee, Large-area growth of MoS_2 at temperatures compatible with integrating back-end-of-line functionality, *2D Materials*, 2020, **8**(2), 025008, DOI: 10.1088/2053-1583/ABC460.

44 W. Mortelmans, S. E. Kazzi, B. Groven, A. N. Mehta, Y. Balaji, S. D. Gendt, M. Heyns and C. Merckling, Epitaxial registry and crystallinity of MoS_2 via molecular beam and metalorganic vapor phase van der Waals epitaxy, *Appl. Phys. Lett.*, 2020, **117**(3), 033101, DOI: 10.1063/5.0013391.

45 S. E. Kazzi, W. Mortelmans, T. Nuytten, J. Meersschaut, P. Carolan, L. Landeloos, T. Conard, I. Radu, M. Heyns and C. Merckling, MoS_2 synthesis by gas source MBE for transition metal dichalcogenides integration on large scale substrates, *J. Appl. Phys.*, 2018, **123**(13), 135702, DOI: 10.1063/1.5008933.

46 D. Chiappe, J. Ludwig, A. Leonhardt, S. E. Kazzi, A. N. Mehta, T. Nuytten, U. Celano, S. Sutar, G. Pourtois, M. Caymax, K. Paredis, W. Vandervorst, D. Lin, S. D. Gendt, K. Barla, C. Huyghebaert, I. Asselberghs and I. Radu, Layer-controlled epitaxy of 2D semiconductors: bridging nanoscale phenomena to wafer-scale uniformity, *Nanotechnology*, 2018, **29**(42), 425602, DOI: 10.1088/1361-6528/AAD798.

47 M. Seol, M.-H. Lee, H. Kim, K. W. Shin, Y. Cho, I. Jeon, M. Jeong, H.-I. Lee, J. Park, H.-J. Shin, M. Seol, M.-H. Lee, H. Kim, K. W. Shin, Y. Cho, I. Jeon, M. Jeong, H.-I. Lee, H.-J. Shin and J. Park, High-Throughput Growth of Wafer-Scale Monolayer Transition Metal Dichalcogenide via Vertical Ostwald Ripening, *Adv. Mater.*, 2020, **32**(42), 2003542, DOI: 10.1002/ADMA.202003542.

48 A. Cohen, A. Patsha, P. K. Mohapatra, M. Kazes, K. Ranganathan, L. Houben, D. Oron and A. Ismach, Growth-Etch Metal-Organic Chemical Vapor Deposition Approach of WS2 Atomic Layers, *ACS Nano*, 2021, **15**(1), 526–538, DOI: 10.1021/ACSNANO.0C05394.

49 C. M. Schaefer, J. M. C. Roque, G. Sauthier, J. Bousquet, C. Hébert, J. R. Sperling, A. Pérez-Tomás, J. Santiso, E. d. Corro and J. A. Garrido, Carbon Incorporation in MOCVD of MoS_2 Thin Films Grown from an Organosulfide Precursor, *Chem. Mater.*, 2021, **33**(12), 4474–4487, DOI: 10.1021/ACS.CHEMMATER.1C00646.

50 J. Mun, Y. Kim, I. S. Kang, S. K. Lim, S. J. Lee, J. W. Kim, H. M. Park, T. Kim and S. W. Kang, Low-temperature growth of layered molybdenum disulphide with controlled clusters, *Sci. Rep.*, 2016, **6**(1), 1–7, DOI: 10.1038/srep21854.

51 J. Zhou, J. Lin, X. Huang, Y. Zhou, Y. Chen, J. Xia, H. Wang, Y. Xie, H. Yu, J. Lei, D. Wu, F. Liu, Q. Fu, Q. Zeng, C. H. Hsu, C. Yang, L. Lu, T. Yu, Z. Shen, H. Lin, B. I. Yakobson, Q. Liu, K. Suenaga, G. Liu and Z. Liu, A library of atomically thin metal chalcogenides, *Nature*, 2018, **556**(7701), 355–359, DOI: 10.1038/s41586-018-0008-3.

52 K. Zhang, B. M. Bersch, F. Zhang, N. C. Briggs, S. Subramanian, K. Xu, M. Chubarov, K. Wang, J. O. Lerach, J. M. Redwing, S. K. FullertonShirey, M. Terrones and J. A. Robinson, Considerations for Utilizing Sodium Chloride in Epitaxial Molybdenum

Disulfide, *ACS Appl. Mater. Interfaces*, 2018, **10**(47), 40831–40837, DOI: **10.1021/ACSAMI.8B16374**.

53 S. Boandoh, S. H. Choi, J.-H. Park, S. Y. Park, S. Bang, M. S. Jeong, J. S. Lee, H. J. Kim, W. Yang, J.-Y. Choi, S. M. Kim and K. K. Kim, A Novel and Facile Route to Synthesize Atomic-Layered MoS_2 Film for Large-Area Electronics, *Small*, 2017, **13**(39), 1701306, DOI: **10.1002/smll.201701306**.

54 S. H. Choi, B. Stephen, J. H. Park, J. S. Lee, S. M. Kim, W. Yang and K. K. Kim, Water-Assisted Synthesis of Molybdenum Disulfide Film with Single Organic Liquid Precursor, *Sci. Rep.*, 2017, **7**(1), 1–8, DOI: **10.1038/s41598-017-02228-8**.

55 H. Li, From bulk to monolayer MoS_2: evolution of Raman scattering, *Adv. Funct. Mater.*, 2012, **22**(7), 1385–1390, DOI: **10.1002/adfm.201102111**.

56 K. Zhang, N. J. Borys, B. M. Bersch, G. R. Bhimanapati, K. Xu, B. Wang, K. Wang, M. Labella, T. A. Williams, M. A. Haque, E. S. Barnard, S. Fullerton-Shirey, P. J. Schuck and J. A. Robinson, Deconvoluting the Photonic and Electronic Response of 2D Materials: The Case of MoS_2, *Sci. Rep.*, 2017, **7**(1), 1–8, DOI: **10.1038/s41598-017-16970-6**.

57 S. Shree, A. George, T. Lehnert, C. Neumann, M. Benelajla, C. Robert, X. Marie, K. Watanabe, T. Taniguchi, U. Kaiser, B. Urbaszek and A. Turchanin, High optical quality of MoS_2 monolayers grown by chemical vapor deposition, *2D Materials*, 2019, **7**(1), 015011, DOI: **10.1088/2053-1583/AB4F1F**.

58 H. P. Komsa, J. Kotakoski, S. Kurasch, O. Lehtinen, U. Kaiser and A. V. Krasheninnikov, Two-dimensional transition metal dichalcogenides under electron irradiation: defect production and doping, *Phys. Rev. Lett.*, 2012, **109**(3), 035503, DOI: **10.1103/PHYSREVLETT.109.035503/FIGURES/5/MEDIUM**.